



Vacancy defects in a stress-corrosion-cracked Type 304 stainless steel investigated by positron annihilation spectroscopy

A. Yabuuchi*, M. Maekawa, A. Kawasuso

Advanced Science Research Center, Japan Atomic Energy Agency, 1233 Watanuki, Takasaki, Gunma 370-1292, Japan

ARTICLE INFO

Article history:

Received 26 May 2011

Accepted 3 August 2011

Available online 22 August 2011

ABSTRACT

To reveal vacancy formation during the stress corrosion cracking (SCC), three factors influencing SCC in Type 304 stainless steels—sensitization heat treatment, corrosion treatment and tensile plastic deformation—were investigated by means of positron annihilation spectroscopy. Vacancy defects induced by the sensitization heat treatment and by tensile deformation were identified as monovacancies. These monovacancies were annealed within the same temperature range in which light water reactors are operated (280–320 °C). The above results allow us to conclude that such vacancy defects play an important role in high-temperature-water SCC crack propagation.

© 2011 Elsevier B.V. All rights reserved.

1. Introduction

Stainless steels are generally highly resistant to corrosion, owing to the formation of a stable chromium oxide barrier. Upon heating at 450–800 °C, however, the corrosion resistance of stainless steels deteriorates markedly. This is due to the formation of chromium carbide (Cr_{23}C_6) at grain boundaries and an associated reduction of available chromium atoms for oxide barrier formation. This phenomenon is called sensitization. In 1970s, it was reported that stress corrosion cracking (SCC) occurs when both stress and corrosion conditions are jointly conducive to it. Therefore, from the 1980s, low-carbon stainless steels, in which sensitization rarely occurs, have been used as nuclear reactor materials; indeed, SCC-induced failures have been substantially reduced. Even so, however, such failures have not been completely avoided, even in low-carbon stainless steels. This suggests that there are still important factors behind SCC failures that are not sufficiently suppressed by simply improving corrosion resistance. Thus, the mechanism for SCC within stainless steels is an important research topic, particularly with regards to such critical applications as long-term use in light water nuclear reactors.

Recently, a hypothesis that SCC crack propagation is mediated by atomic vacancies under a stress gradient at the crack tip has been proposed [1–3].

Positron annihilation spectroscopy offers a unique approach to studying vacancy defects. It is based on the tendency for positrons implanted into a solid to become trapped by vacancy defects and annihilate with electrons to emit 511 keV gamma-rays. Such annihilation gamma-rays convey information about the vacancy defects from which they originated. In the present study, Type

304 stainless steels subjected to sensitization heat treatment, corrosion treatment, and tensile plastic deformation were examined by means of positron annihilation spectroscopy to elucidate vacancy formation during SCC.

2. Experimental

The samples used in this study were commercially available Type 304 stainless steel foils or sheets with a thickness of 0.05 mm or 1 mm. To suppress chromium carbide precipitation, all the samples were annealed at 1150 °C for 2 h in vacuum silica tube and subsequently quenched into ice water. The above heat treatment is called solution annealing. With regards to the thick samples, this state was defined as the initial (reference) state. For the thin samples, an additional annealing step was carried out at 400 °C for 30 min to remove quenched-in thermal equilibrium vacancies. Both the thin and thick samples were then separately subjected to the following: (i) sensitization heat treatment at 650 °C for 24 h in vacuum, (ii) plastic deformation up to a strain of 14% under a 150 MPa tensile stress at room temperature, (iii) a corrosion treatment in boiling water containing 35% MgCl_2 at approximately 130 °C for 72 h, and (iv) irradiation with 2 MeV electrons to a dose of $3 \times 10^{18} \text{ e}^-/\text{cm}^2$ at a temperature below 60 °C. Finally, to investigate the thermal stability of defects induced by these treatments, the samples were isochronally annealed in vacuum with a temperature step of 100 °C and a duration of 30 min. After each annealing step, the samples were quenched into ice water.

Positron annihilation measurements were conducted using a positron microbeam (energy: 20 keV; spot size: 20 μm) [4], an energy-variable positron beam (energy: 0.2–30 keV; spot size: 5 mm), and a conventional positron source ($^{22}\text{NaCl}$, 700 kBq) deposited onto a titanium foil (thickness: 5 μm). In the positron

* Corresponding author. Tel.: +81 27 346 9330; fax: +81 27 346 9432.

E-mail address: yabuuchi.atsushi@jaea.go.jp (A. Yabuuchi).

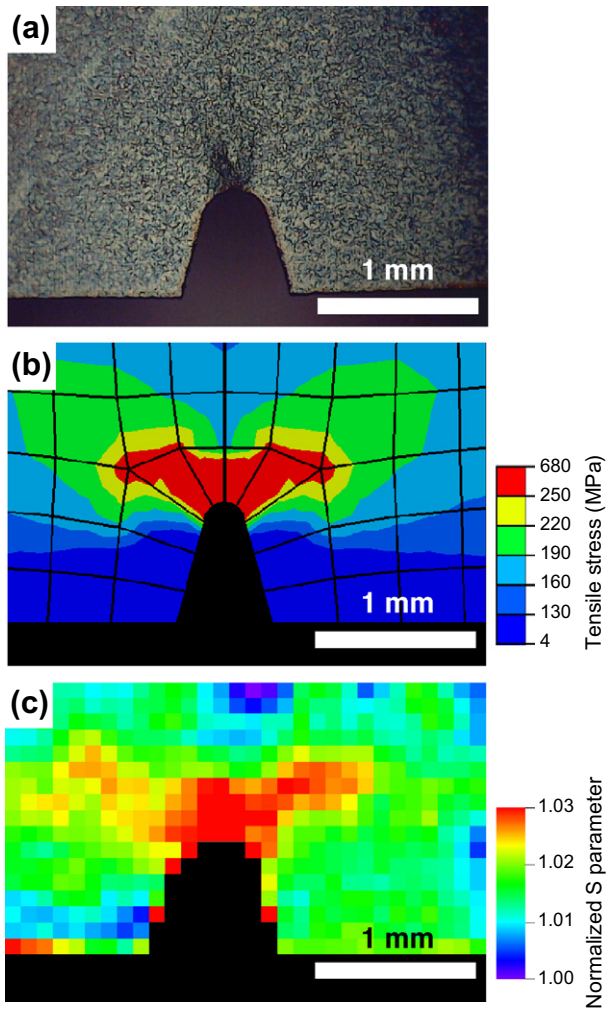


Fig. 1. (a) Optical microscope image, (b) tensile stress distribution calculated using the ABAQUS code, and (c) S parameter mapping with a pixel size of $100 \times 100 \mu\text{m}^2$, obtained under a tensile stress of approximately 150 MPa in the horizontal direction.

beam experiments, Doppler broadening of the annihilation radiation (DBAR) measurements were carried out using a high-purity germanium detector. To monitor the presence of vacancy defects, the DBAR spectra thus obtained were characterized in terms of an S parameter, which is defined as the peak intensity. All the S parameters were normalized to those obtained for the initial state. Positron annihilation lifetime measurements were performed using the positron source and a fast-fast spectrometer with a time resolution of 245 ps (full width at half-maximum, FWHM).

3. Results and discussion

3.1. SCC propagation

Fig. 1a shows an optical microscope image of a notched and solution-annealed sample (thickness: 0.05 mm). A tensile stress of approximately 150 MPa is applied horizontally relative to the figure. This is less than the yield stress of Type 304 stainless steels (250 MPa). However, as shown in Fig. 1b, finite-element analysis (ABAQUS code) shows that tensile stress concentrates at the notch tip. This concentration is such that in the red¹ region, tensile stress

would be greater than 250 MPa and hence plastic deformation would be expected to occur. Fig. 1c shows scanning DBAR measurements as taken with the positron microbeam over the same region as Fig. 1a. Although the S parameter does not increase significantly within the low stress regions beside the notch, it does increase along with the stress gradient emanating from the notch tip as shown in Fig. 1b. This fact implies that vacancy defects are introduced by local plastic deformation caused by the stress concentration.

Fig. 2a and b shows the optical microscope image and S parameter image, respectively, obtained after SCC propagation. Over a 200–400 μm range from the SCC crack, the S parameter clearly increases. Observing Fig. 1c, we note that plastic deformation successively occurs at the crack tip during crack propagation. Since the temperature of boiling MgCl_2 water ($\sim 130^\circ\text{C}$) is lower than the annealing temperature of vacancy defects induced by plastic deformation as discussed in Section 3.6, we also note that most vacancy defects survive during SCC propagation.

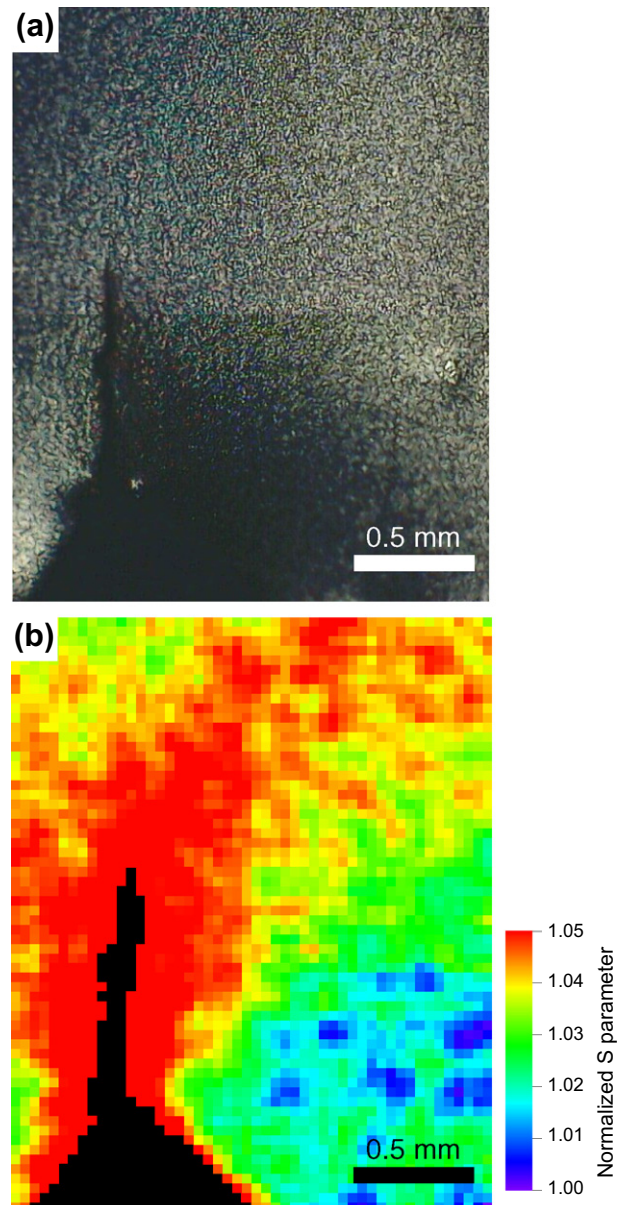


Fig. 2. (a) Optical microscope image and (b) S parameter mapping with a pixel size of $40 \times 40 \mu\text{m}^2$ obtained for a sensitized sample after SCC treatment.

¹ For interpretation of color in Figs. 1 and 2, the reader is referred to the web version of this article.

3.2. Effect of sensitization heat treatment

Fig. 3 shows the S parameter as a function of incident positron energy before and after sensitization heat treatment. Mean positron implantation depth is also shown on the top horizontal axis. The increase in S parameter in the low positron energy region ($E < 5$ keV) is related to surface effects [5,6] and not to the sensitization heat treatment. At $E > 10$ keV, the S parameter of the sensitized sample is sufficiently higher than that of the unsensitized sample. This suggests that vacancy defects are introduced by the sensitization heat treatment. The solid lines shown in the figure show the results of an analysis based on a one-dimensional positron diffusion model using a VEPFIT code [7,8]. The positron diffusion lengths before and after the sensitization heat treatment were 80 nm and 22 nm, respectively. This also indicates an introduction of vacancy defects.

Vacancy defects observed after the sensitization heat treatment are probably generated by the Kirkendall effect. It is known that the inverse Kirkendall effect leads to chromium depletion near the grain boundaries within the irradiation-assisted stress corrosion cracking (IASCC) [9–14]. This migration of irradiation-induced vacancies to grain boundaries results in a corresponding migration of chromium atoms in the opposite direction. Consequently, chromium depletion occurs near the grain boundaries. In a sensitization heat treatment, chromium depletion also occurs near the grain boundaries because of the formation of Cr_{23}C_6 precipitates. Such a chromium concentration gradient causes a migration of the chromium atoms toward the grain boundaries (by the Kirkendall effect) and a flow of vacancies into the grains.

An alternative explanation for the increase in the S parameter after sensitization heat treatment is an introduction of misfit dislocations at precipitate interfaces as reported for Ti-doped austenitic stainless steels in which TiC precipitation occurs inside grains [15]. Note, however, that Cr_{23}C_6 precipitates are formed at grain boundaries in Type 304 stainless steels and that the grain diameter of the samples is approximately 50 μm , which is far larger than the positron diffusion length. Therefore, nearly all positrons would be expected to annihilate inside the grains. That is, the increase in the S parameter might not be attributable to misfit dislocations accompanying the Cr_{23}C_6 precipitates.

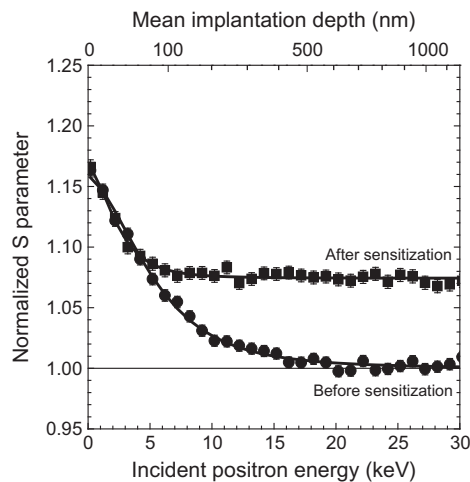


Fig. 3. S parameter as a function of incident positron energy obtained before (filled circles) and after (filled squares) sensitization heat treatment. Solid lines are fitting curves calculated using VEPFIT code.

3.3. Plastic deformation under tensile stress

To estimate the concentration of vacancy defects induced by a stress concentration as shown in Fig. 1b, a tensile deformation test was performed. Fig. 4 shows the change in the S parameter for foil tensile test pieces during tensile deformation. It is seen that the S parameter monotonically increases with strain. This indicates an introduction of vacancy defects by plastic deformation. From a comparison of the electron-irradiated sample and its annealing process (see Sections 3.5 and 3.6), it is shown that monovacancies are mainly responsible for positron trapping in a plastically deformed sample. Here, the S parameter may be given by $S = (1 - f)S_B + f S_V$, where S_B and S_V are S parameters for the bulk ($=1.000$) and vacancy defects, f is the annihilation fraction of positrons at vacancy defects ($= \mu C_V / (\tau_B^{-1} + \mu C_V)$), and μ and C_V are the specific trapping rate and the concentration, respectively, of vacancy defects. As shown in Section 3.5, $\tau_B = 102$ ps and $S_V = 1.127$ for monovacancies. The vacancy concentration introduced by plastic deformation is phenomenologically given by $C_V = \eta \epsilon^n$, where η and n are constants and ϵ is strain [16]. The solid line in Fig. 4 is the calculated S parameter as given by the above equations with fitting parameters of $\mu\eta (=1.4 \times 10^{10} \text{ s}^{-1})$ and $n (=0.6)$. Under an assumption that the specific trapping rate of a monovacancy in Type 304 stainless steel is similar to that in pure Fe ($1.1 \times 10^{15} \text{ s}^{-1}$) [17], the vacancy concentration is estimated to be 3×10^{-6} at $\epsilon = 10\%$. Subsequently, we estimate the vacancy concentration at the notch tip shown in Fig. 1. C_V can be described as $C_V = (S - S_B) / \tau_B \mu (S_V - S)$ by transforming the above-mentioned formulae. $S = 1.03$ is observed at the notch tip as shown in Fig. 1c. Consequently, the vacancy concentration of that region is estimated to be 3×10^{-6} . From the result of the tensile test, this corresponds to the tensile deformation at $\epsilon = 10\%$. Incidentally, recent EBSD studies have revealed that approximately 10% of localized tensile strain is distributed near grain boundaries around SCC cracks [18,19]. The observed result of S parameter at the notch tip is consistent with the results of recent EBSD studies. These results imply that a high concentration of vacancy defects is introduced around SCC cracks.

3.4. Effect of corrosion treatment

As shown in Fig. 5, the S parameter increases in the sub-surface region (up to 50 nm) upon a corrosion treatment after sensitization heat treatment. A detailed VEPFIT analysis indicated that this modulated layer thickness and its S parameter were 12 nm and 1.250, respectively. These results imply that some porous structures, such as an oxide layer (Fe_3O_4) [20], are induced by the corrosion treatment. At $E > 15$ keV, the S parameter slightly decreases upon a corrosion treatment. Considering the fact that the corrosion treatment

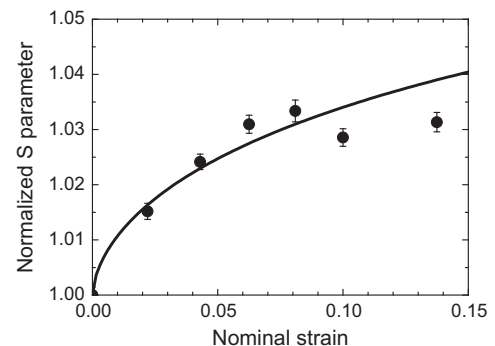


Fig. 4. S parameter as a function of tensile strain. Solid line is the fitting curve calculated using equations described in the text.

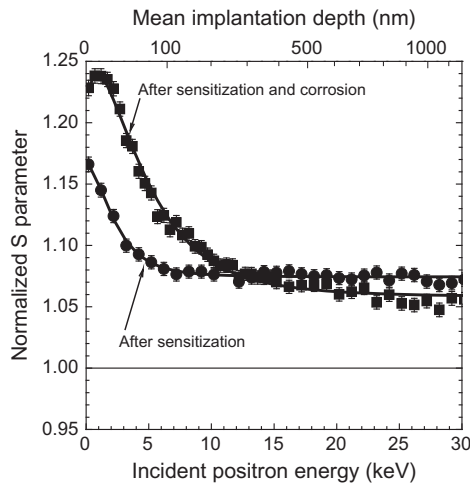


Fig. 5. S parameter as a function of incident positron energy obtained before (filled circles) and after (filled squares) corrosion treatment. Solid lines are fitting curves calculated using the VEPFIT code.

was carried out at approximately 130 °C, the decrease of the S parameter in the deeper region can be explained as a partial annealing of the sensitization-induced vacancies as discussed in Section 3.6.

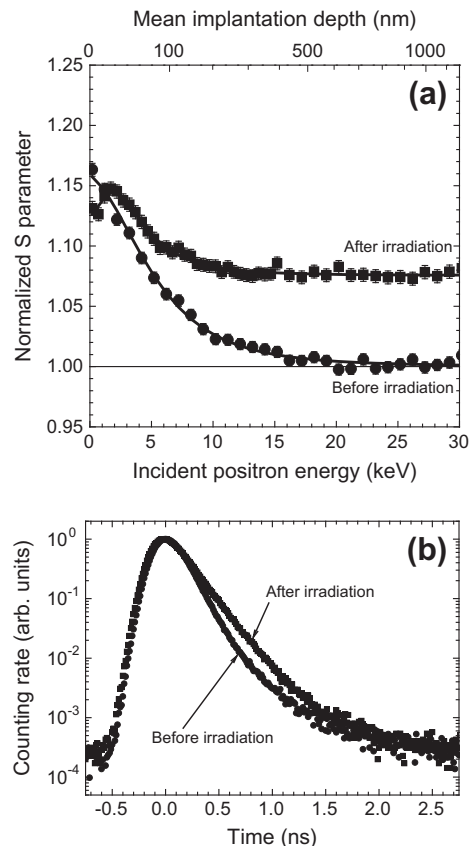


Fig. 6. (a) S parameter as a function of incident positron energy and (b) positron annihilation lifetime spectra obtained before (filled circles) and after (filled squares) electron irradiation to a dose of $3 \times 10^{18} \text{ e}^-/\text{cm}^2$. Solid lines are fitting curves calculated using VEPFIT code.

3.5. Comparison with electron irradiation

Fig. 6a and b shows the S parameter as a function of incident positron energy and positron annihilation lifetime spectra, respectively, before and after electron irradiation. A VEPFIT analysis suggested that the S parameter and the positron diffusion length of the irradiated layer are $S = 1.076$ and $L = 39 \text{ nm}$, respectively. A single positron lifetime of 102 ps was obtained for the unirradiated sample. Upon electron irradiation, two positron lifetime components ($\tau_1 = 57 \text{ ps}$ and $I_1 = 22\%$, $\tau_2 = 177 \text{ ps}$ and $I_2 = 78\%$) were obtained. The second component is related to vacancy defects introduced by irradiation. Taking $\mu_{C_V} = (I_2/I_1)(1/\tau_B - 1/\tau_V) = 14.7 \text{ ns}^{-1}$, the S parameter of the vacancy defects is determined to be $S_V = 1.127$ in a way similar to that described in Section 3.3. Fig. 7 shows an experimental DBAR spectrum obtained after electron irradiation. To see the detailed spectrum shape, the original spectra are divided point-by-point by the spectrum for the reference sample. The spectrum shape exhibits a typical feature for vacancy defects.

From previous studies on metals [21,22], the above positron lifetime ($\tau_2 = 177 \text{ ps}$) seems to be attributable to monovacancies. To confirm this inference, theoretical calculations were conducted based on the atomic superposition method developed by Puska et al. [23]. Also, DBAR spectra were calculated based on the two-component density functional theory. In the calculations, the crystal structure, the lattice constant and the alloy composition are assumed to be face-centered cubic (fcc), 3.593 Å and Fe/Cr/Ni = 0.73/0.19/0.08, respectively. The details of the calculations are described elsewhere [24,25]. The calculated positron lifetimes for the bulk, monovacancy and divacancy in a Type 304 stainless steel were 101 ps, 176 ps and 194 ps, respectively. The solid line in Fig. 7 is the calculated DBAR spectrum for a monovacancy. The observed positron lifetime before irradiation (102 ps) agrees well with the calculated bulk lifetime. Thus, before irradiation, the concentration of vacancy defects is under the detection limit ($<10^{-7}$). The observed second lifetime ($\tau_2 = 177 \text{ ps}$) and the DBAR spectrum are in good agreement with those calculated for a monovacancy. Thus, vacancy defects induced by the electron irradiation can be identified as monovacancies and not as further vacancy clusters. In pure iron, monovacancies are not stable at room temperature [26]. Monovacancies in stainless steels might be stable because of the crystal structure and/or composition of those alloys [27–30].

As seen in Fig. 7, the DBAR spectra after the sensitization heat treatment and plastic deformation are in good agreement with that after the electron irradiation. This suggests that monovacancies are

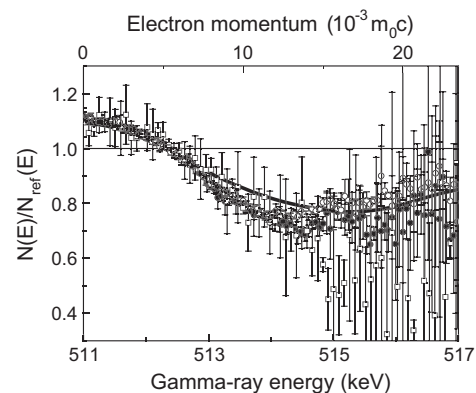


Fig. 7. DBAR spectra obtained after electron irradiation to a dose of $3 \times 10^{18} \text{ e}^-/\text{cm}^2$ (filled circles), sensitization treatment at 650 °C for 24 h (open circles) and plastic deformation at a strain of 14% (open squares). The spectrum amplitude of the plastic deformation is adjusted by a factor of 2.5. All these spectra are differentiated by the spectrum for the reference sample. Solid line is the theoretical DBAR spectrum for a monovacancy in Type 304 stainless steel.

responsible for positron trapping in these samples, too. However, the spectrum after the plastic deformation looks partially different from the other spectra at high gamma-ray energy region. It is known that dislocation acts as shallow positron trap in materials [31]. The plastic deformed sample differs from other samples in that high density dislocations are included. Therefore, it is inferred that implanted positrons in the plastic deformed sample were trapped at vacancies and dislocations. We consider that the difference of the spectrum shape at high-energy region is attributed to the positrons annihilated at dislocations.

3.6. Annealing properties

To reveal the thermal stabilities of vacancy defects within the above samples, we also investigate annealing process. Fig. 8 shows S parameters for samples after sensitization heat treatment, tensile deformation, and electron irradiation as a function of annealing temperature. It is found that these S parameters commonly decrease to the initial level in the temperature range of 200–400 °C, again increase in the range of 600–900 °C and subsequently decrease toward 1000 °C. The first recovery at 200–400 °C is explainable as a disappearance of monovacancies. The increase in S parameters at 600–900 °C may be attributed to a re-introduction of vacancy defects due to sensitization as described in Section 3.2. This temperature range is corresponding to a temperature where austenitic stainless steels are sensitized. The decrease of S parameters toward 1000 °C for the sensitization heat-treated and the electron-irradiated samples indicates re-solution. The S parameter of the tensile deformed sample does not decrease above 1000 °C. In this study, stainless steel foils with a thickness of 0.05 mm were used for the tensile-deformed sample while stainless steel sheets with a thickness of 1 mm were used for the sensitization heat-treated and the electron-irradiated samples. Thus, the cooling rate of the tensile-deformed sample is more rapid than that of the other samples. We consider that the increase in S parameter at 600–900 °C is caused by sensitization effect and the keeping of high S parameter for the tensile deformed sample quenched from 1000 °C is caused by freezing thermal equilibrium vacancies which existed at 1000 °C. It is reported that positrons begin to detect thermal equilibrium vacancies of austenitic stainless steels from 900 °C [32]. Indeed, the S parameter of undeformed foil sample which is quenched from 1000 °C is higher than that of the reference sample, and decreases when it is annealed at 400 °C. This shows that thermal equilibrium vacancies are frozen in the quenched foil sample. In a previous positron annihilation lifetime

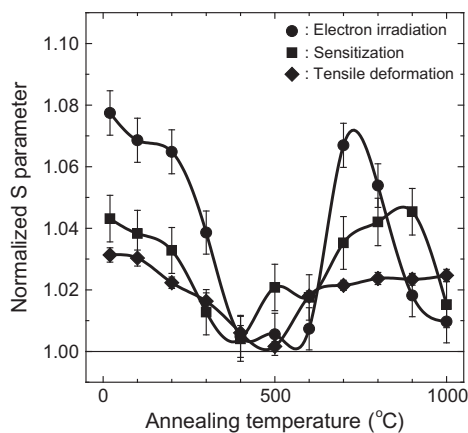


Fig. 8. S parameter for sensitization heat treated (filled squares), tensile deformed (filled diamonds) and electron irradiated (filled circles) samples as a function of annealing temperature.

spectroscopy study, it is reported that a large amount of monovacancy is detected from the electron-irradiated Fe–0.2 wt% C, Fe–0.5 wt% Si, Fe–1.5 wt% Mn and Fe–0.3 wt% Cu dilute alloys while only a small amount of vacancy cluster is detected from the electron-irradiated pure-Fe [33]. It indicates strong interactions between the vacancies and the solute atoms. Therefore, it is thought that thermal equilibrium vacancies which existed in the stainless steel foil at 1000 °C are trapped by impurity atoms like C, Mn or Si atoms during quenching and stabilized without clustering at room temperature.

The first recovery of S parameters (200–400 °C) corresponds to a light water reactor operating temperature. That is, monovacancies in stainless steels are mobile at reactor operating temperature. This indicates a possibility that monovacancies accumulate at crack tip grain boundaries, resulting in the development of tight cracks.

Fig. 9a shows S parameters as a function of incident positron energy obtained after the corrosion treatment. Fig. 9b shows the result of VEPFIT analyses with two-layer model. It is found that upon annealing, the S parameter gradually decreases at 0–3 keV and that the layer thickness increases with increasing annealing temperature. The corrosion-induced layer still remains at 600 °C. This indicates that the increase in the S parameter in the corrosion-induced layer is not caused by the formation of monovacancies.

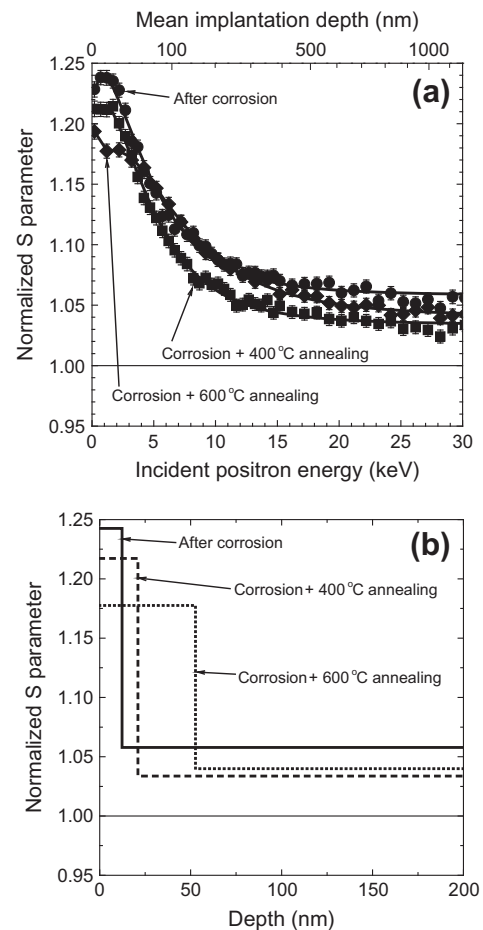


Fig. 9. (a) S parameter as a function of incident positron energy after corrosion treatment (filled circles) and subsequent annealing at 400 °C (filled squares) or 600 °C (filled diamonds). Solid lines are fitting curves calculated using VEPFIT code. (b) Depth profiles of S parameters obtained through VEPFIT analyses for the above samples.

4. Conclusions

We utilized positron annihilation spectroscopy to examine three factors influencing SCC in Type 304 stainless steels—sensitization heat treatment, corrosion treatment and tensile plastic deformation. A thin porous layer was found to be formed upon the corrosion treatment. However, it is not clear if mobile vacancy defects are involved there. Major sources of vacancy defects are the plastic deformation and, during the sensitization heat treatment, the Kirkendall effect. These vacancy defects are monovacancies and are annealed at 200–400 °C. This recovery temperature corresponds to the light water reactor operating temperatures (280–320 °C). It has thus been suggested that monovacancies play an important role in the high-temperature-water SCC crack propagation mechanism.

Acknowledgements

This study was carried out as part of the project “In situ analysis of crack tips in stainless steels under tensile stress”, entrusted to the Japan Atomic Energy Agency (JAEA) by the Ministry of Education, Culture, Sports, Science and Technology of Japan (MEXT) and was partially supported by a MEXT Grant-in-Aid for Young Scientists (B), No. 22760682, 2010. The electron irradiation experiments were performed using the Takasaki-JAEA facility.

References

- [1] R.W. Staehle, in: Proceedings of the International Conference on Water Chemistry of Nuclear Reactor Systems, Jeju Island, Korea, 2006.
- [2] K. Arioka, T. Yamada, T. Terachi, T. Miyamoto, Corrosion 64 (2008) 691.
- [3] K. Arioka, T. Miyamoto, T. Yamada, T. Terachi, Corrosion 66 (2010) 015008.
- [4] M. Maekawa, A. Kawasuso, Applied Surface Science 255 (2008) 39.
- [5] A.P. Mills Jr., Physical Review Letters 41 (1978) 1828.
- [6] P.J. Schultz, K.G. Lynn, Reviews of Modern Physics 60 (1988) 701.
- [7] A. Van Veen, H. Schut, J. De Vries, R.A. Hakvoort, M.R. Ijpm, AIP Conference Proceedings 218 (1990) 171.
- [8] A. van Veen, H. Schut, M. Clement, J.M.M. de Nijs, A. Kruseman, M.R. Ijpm, Applied Surface Science 85 (1995) 216.
- [9] A.D. Marwick, Journal of Physics F: Metal Physics 8 (1978) 1849.
- [10] E.A. Kenik, R.H. Jones, G.E.C. Bell, Journal of Nuclear Materials 212–215 (1994) 52.
- [11] T.R. Allen, G.S. Was, E.A. Kenik, Journal of Nuclear Materials 244 (1997) 278.
- [12] T.R. Allen, J.T. Busby, G.S. Was, E.A. Kenik, Journal of Nuclear Materials 255 (1998) 44.
- [13] T.R. Allen, G.S. Was, Acta Materials 46 (1998) 3679.
- [14] S.M. Bruemmer, E.P. Simonen, P.M. Scott, P.L. Andresen, G.S. Was, J.L. Nelson, Journal of Nuclear Materials 274 (1999) 299.
- [15] J. Arunkumar, S. Abhaya, R. Rajaraman, G. Amarendra, K.G.M. Nair, C.S. Sundar, Baldev Raj, Journal of Nuclear Materials 384 (2009) 245.
- [16] B. Russell, Philosophical Magazine 88 (1963) 615.
- [17] Y.-K. Park, J.T. Waber, M. Meshii, C.L. Snead Jr., C.G. Park, Physical Review B 34 (1986) 823.
- [18] M. Kamaya, A.J. Wilkinson, J.M. Titchmarsh, Nuclear Engineering Design 235 (2005) 713.
- [19] Y. Kaji, Y. Miwa, T. Tsukada, M. Hayakawa, N. Nagashima, JAEA-Res, 2007-008.
- [20] P. Ampornrat, C.B. Bahn, G.S. Was, in: Proceedings of the 12th International Conference on Environmental Degradation Materials in Nuclear Power Systems, Salt Lake City, USA, 2005.
- [21] P. Hautojärvi, T. Judin, A. Vehanen, J. Yli-Kauppila, J. Johansson, J. Verdone, P. Moser, Solid State Communications 29 (1979) 855.
- [22] A. Vehanen, P. Hautojärvi, J. Johansson, J. Yli-Kauppila, P. Moser, Physical Review B 25 (1982) 762.
- [23] M.J. Puska, R.M. Nieminen, Reviews of Modern Physics 66 (1994) 841.
- [24] A. Kawasuso, H. Arshima, M. Maekawa, H. Itoh, T. Kabutomori, Journal of Alloys Compound 486 (2009) 278.
- [25] A. Kawasuso, M. Maekawa, K. Betsuyaku, Journal of Physics: Conference Series 225 (2010) 012027.
- [26] E. Kuramoto, H. Abe, M. Takenaka, F. Hori, Y. Kamimura, M. Kimura, K. Ueno, Journal of Nuclear Materials 239 (1996) 54.
- [27] H. Watanabe, E. Kuramoto, N. Yoshida, Transactions in Japan Institute of Metals 29 (1988) 769.
- [28] C.L. Gil, A.P. de Lima, N.A. de Campos, P. Sperr, G. Kögel, W. Triftshäuser, Radiation Effects and Defects in Solids 112 (1990) 111.
- [29] J. Dryzek, C. Wesseling, E. Dryzek, B. Cleff, Materials Letters 21 (1994) 209.
- [30] P. Asoka-Kumar, J.H. Hartley, R.H. Howell, P.A. Sterne, D. Akers, V. Shah, A. Denison, Acta Materials 50 (2002) 1761.
- [31] H. Häkkinen, S. Mäkinen, M. Manninen, Physical Review B 41 (1990) 12441.
- [32] S.M. Kim, W.J.L. Buyers, Canadian Journal of Physics 61 (1983) 140.
- [33] Y. Nagai, K. Takadate, Z. Tang, H. Ohkubo, H. Sunaga, H. Takizawa, M. Hasegawa, Physical Review B 67 (2003) 224202.